Int. J. Heat Mass Transfer. Vol. 24, No. 4, pp. 649–657, 1981
Printed in Great Britain

0017–9310/81/040649–09 $02.00/0
Pergamon Press Ltd

NUMERICAL INVESTIGATION OF SUPERSONIC NON-EQUILIBRIUM CARBON DIOXIDE FLOW PAST BLUNT BODIES

YU. P. GOLOVACHOV
A. F. Ioffe Physical-Technical Institute, Leningrad, U.S.S.R.

(*Received* 20 *March* 1980)

Abstract—Non-equilibrium axisymmetric flow about spherically blunted cones is considered on the basis of the Navier–Stokes equations. Vibrational relaxation of carbon dioxide molecules, non-equilibrium chemistry and radiative energy transfer are taken into account. The solutions are obtained numerically with the use of implicit finite-difference schemes. The effect of nitrogen, argon and sodium impurities on the shock layer parameters is investigated.

NOMENCLATURE

t, time;
p, pressure;
T, translational temperature;
T^*, effective temperature of electronic excitation;
h, specific enthalpy;
C, mass fraction;
E, specific vibrational energy of carbon dioxide molecules;
E^*, energy of excited electronic state;
s, distance along the body surface;
n, normal distance from the body surface;
u, v, velocity components in s, n directions;
r, distance between the symmetry axis and the body surface;
m, molecular weight;
a, body nose radius;
Re, Reynolds number;
Sc, Schmidt number;
R, universal gas constant;
k, Boltzmann constant;
N, number of mixture components;
q_c, convective heat flux;
q_r, radiative heat flux;
C_f, skin friction coefficient;
N_e, number density of electrons;
g, degeneracy.

Greek symbols

ρ, density;
ω, mass production rate;
κ, curvature of generatrix of the body surface;
θ, angle between generatrix and free stream direction;
θ_c, cone half-angle;
μ, viscosity;
λ, thermal conductivity;
τ_v, vibrational relaxation time;
ε, shock wave distance from the body surface.

Subscripts

∞, free stream;
w, wall;
i, ith species;
eq, equilibrium value.

Superscripts

$*$, excited state;
^{0}, ground state.

1. INTRODUCTION

AT HYPERSONIC velocities the flow field about a blunt body is influenced to a great extent by various physical and chemical processes. With reduction in the gas density, the relaxation times of these processes become comparable with the characteristic flow time and this dictates the necessity of allowing for the non-equilibrium effects. Concurrently, diffusion, viscosity and heat conduction grow in importance and they start to influence the entire flow area. Under these conditions, the non-equilibrium flow past blunt bodies should be studied numerically on the basis of the Navier–Stokes equations. This situation is typical, for instance, of the hypersonic flight in the Earth's atmosphere at altitudes 60–90 km.

A non-equilibrium viscous gas flow in the vicinity of the stagnation line was studied by many authors [1–6]. Numerical solutions for axisymmetric flows about the bodies of analytical shape (sphere, hyperboloid) and about spherically blunted cones have been obtained in [7–12]. The majority of these investigations have been carried out for a non-equilibrium flow of air.

The present paper considers a hypersonic carbon dioxide flow past spherically blunted cones with large half-angles under the conditions of entry into the Martian atmosphere (v_∞ = 4000–7000 m/s, ρ_∞ = 10^{-5}–10^{-2} kg/m^3). The flow field on the upstream side of the bodies, convective and radiative heat

transfer in the shock layer and non-equilibrium ionization are investigated. Under the conditions stated, the effects of ionization and radiation on the flow field parameters are rather small and therefore they are not allowed for in the calculation of gasdynamic functions and concentrations of neutral species. These results are then used to estimate the upper limit of the non-equilibrium radiative heat flux to the body surface and to study the shock layer ionization.

2. ANALYSIS OF THE FLOW FIELD

The flows considered are characterized by Reynolds numbers $Re \gtrsim 10^2$. Variation of gas parameters occurs mainly across the shock layer. Therefore, in order to simplify the computations, only normal components of mass and energy fluxes caused by diffusion and thermal conduction are included into continuity equations for mixture components and energy conservation equations. Besides, viscous terms are neglected which are by the order of magnitude less than $1/\sqrt{Re}$ throughout the whole shock layer [13].

The governing equations are:

Continuity (for mixture)

$$\frac{\partial \rho}{\partial t} + \frac{\partial}{\partial n}(\rho v) + \frac{1}{1+\kappa n}\frac{\partial}{\partial s}(\rho u) + \rho(g_1 v + g_2 u) = 0; \quad (1)$$

Momentum

$$\frac{\partial v}{\partial t} + v\frac{\partial v}{\partial n} + \frac{1}{\rho}\frac{\partial p}{\partial n} + \frac{u}{1+\varkappa n}\left(\frac{\partial v}{\partial s} - \varkappa u\right) - \frac{1}{3\rho}\left\{4\frac{\partial}{\partial n}\left(\mu\frac{\partial v}{\partial n}\right) + g_2\left(\mu\frac{\partial u}{\partial n} - 2u\frac{\partial \mu}{\partial n}\right) + \frac{1}{1+\varkappa n}\left[3\frac{\partial}{\partial s}\left(\mu\frac{\partial u}{\partial n}\right) - 2\frac{\partial}{\partial n}\left(\mu\frac{\partial u}{\partial s}\right)\right]\right\} = 0, \quad (2)$$

$$\frac{\partial u}{\partial t} + v\frac{\partial u}{\partial n} + \frac{1}{1+\varkappa n}\left[u\left(\frac{\partial u}{\partial s} + \varkappa v\right) + \frac{1}{\rho}\frac{\partial p}{\partial s}\right] - \frac{1}{\rho}\left[\frac{\partial}{\partial n}\left(\mu\frac{\partial u}{\partial n}\right) + g_1\mu\frac{\partial u}{\partial n} - \frac{\varkappa}{1+\varkappa n}u\frac{\partial \mu}{\partial n}\right] = 0; \quad (3)$$

Energy

$$\frac{\partial h}{\partial t} - \frac{1}{\rho}\frac{\partial p}{\partial t} + v\left(\frac{\partial h}{\partial n} - \frac{1}{\rho}\frac{\partial p}{\partial n}\right) + \frac{u}{1+\varkappa n}\left(\frac{\partial h}{\partial s} - \frac{1}{\rho}\frac{\partial p}{\partial s}\right) + \frac{1}{\rho}\left[\frac{\partial}{\partial n}q_n + g_1 q_n + \mu\left(\frac{\partial u}{\partial n} - 2\frac{\varkappa u}{1+\varkappa n}\right)\frac{\partial u}{\partial n}\right] = 0; \quad (4)$$

Vibrational energy of carbon dioxide molecules

$$\frac{\partial E}{\partial t} + v\frac{\partial E}{\partial n} + \frac{u}{1+\varkappa n}\frac{\partial E}{\partial s} - \frac{1}{\rho} \times \left[\frac{\partial}{\partial n}\left(\frac{\mu}{Sc_v}\frac{\partial E}{\partial n}\right) + \frac{\mu}{Sc_v}\frac{\partial E}{\partial n} \times \left(g_1 + 2\frac{\partial}{\partial n}\ln C_{CO_2}\right)\right] + \frac{E - E_{eq}}{\tau_v} = 0; \quad (5)$$

Continuity (for mixture components)

$$\frac{\partial C_i}{\partial t} + v\frac{\partial C_i}{\partial n} + \frac{u}{1+\kappa n}\frac{\partial C_i}{\partial s} - \frac{1}{\rho}\left[\frac{\partial}{\partial n}\left(\frac{\mu}{Sc_i}\frac{\partial C_i}{\partial n}\right) + g_1\frac{\mu}{Sc_i}\frac{\partial C_i}{\partial n}\right] - \frac{\omega_i}{\rho} = 0 \qquad (i = 1, \ldots, N) \quad (6)$$

Here

$$g_1 = \frac{\kappa}{1+\kappa n} + \frac{\cos\theta}{r + n\cos\theta}, \quad g_2 = \frac{\sin\theta}{r + n\cos\theta},$$

$$q_n = -\lambda\frac{\partial T}{\partial n} - \sum_{i=1}^{N} h_i\frac{\mu}{Sc_i}\frac{\partial C_i}{\partial n} - C_{CO_2}\frac{\mu}{Sc_v}\frac{\partial E}{\partial n}.$$

Vibrational relaxation of carbon dioxide molecules is described as follows [14]: it is assumed that first molecular collisions produce excitation of the bending mode and then its energy is instantaneously distributed among all of the vibrational modes. The vibrational relaxation time τ_v is evaluated from the data of [14]. The vibrational degrees of freedom of the remainder molecules as well as the rotational degrees of freedom of all the molecules are assumed to be excited in equilibrium consistent with the translational temperature.

The viscosity and thermal conductivity of the mixture are calculated by the Wilke and Mason–Saxena formulae, with collision integrals being adopted from [15, 16]. In most calculations, multicomponent diffusion is taken into account by means of the constant effective Schmidt number $Sc = 0.5$.

In calculations of pure carbon dioxide and CO_2 + Ar flows about bodies, the following chemical reactions are accounted for:

$$CO_2 + M \rightleftarrows CO + O + M, O_2 + M \rightleftarrows O + O + M,$$

$$CO + M \rightleftarrows C + O + M, \quad CO_2 + O \rightleftarrows CO + O_2,$$

where M denotes any particle of the mixture. The study of CO_2 + N_2 flows is performed with the use of the McKenzie and Arnold chemical model [17] complemented with oxygen molecules. The rate constants are taken from [12, 17, 18].

The flow area considered is bounded by the detached shock wave, symmetry axis, wall and some surface located far enough from the stagnation point. The Rankine–Hugoniot relations modified to account for shock slip effects are used to evaluate the flow parameters behind the shock [19]. Shock thickness is approximately equal to a few mean free paths of molecules. Therefore vibrational excitation processes and chemical reactions are assumed to be frozen within the shock. At the wall boundary the velocity

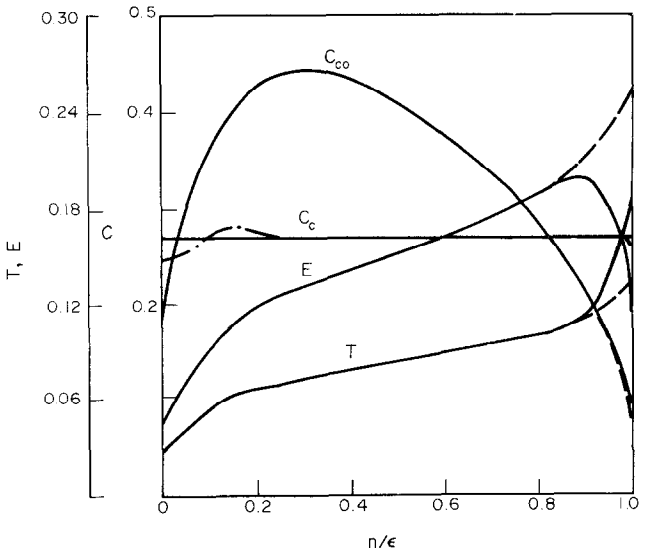

FIG. 1. Profiles of shock layer parameters on the stagnation line for $v_\infty = 6000$ ms; $\rho_\infty = 2 \times 10^{-4}$ kg/m^3; $a = 0.2$ m; $\theta_c = 60°$; $T_w = 2500$ K.

components are assumed to be equal to zero. The wall is regarded as being catalytic and having a constant temperature. The symmetry relations and the backward difference approximations are used on the stagnation line and at the downstream boundary of the flow region considered, respectively.

Stationary flow field parameters are obtained by the time-dependent technique. An implicit finite-difference scheme of the second order accuracy in the spatial coordinates is used. At each time step the non-linear set of finite-difference equations is solved by using the Newton iterative method. In each iteration, it is split into independent subsets along the normals to the body surface. The linear equations along each normal are solved by using the vector elimination method. For full details on the numerical solution and calculation of flows past spherically blunted cones see [20, 21].

The step of integration over s was taken as 0.1745. In most calculations the number of mesh points per each normal s = const was equal to 31. The regions of steep gradients near the shock wave and the body surface are stretched by applying analytical transformation of the normal coordinate [20]. The accuracy of the results

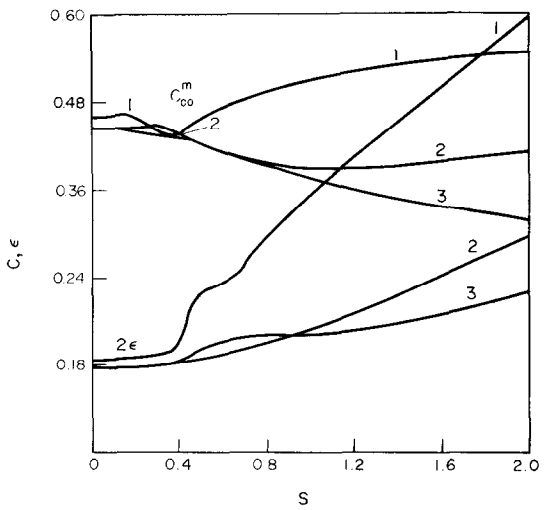

FIG. 2. Variation of shock layer thickness and maximum carbon monoxide concentration along the shock layer for $v_\infty = 6000$ m/s; $\rho_\infty = 2 \times 10^{-4}$ kg/m^3; $a = 0.2$ m; $T_w = 2500$ K.

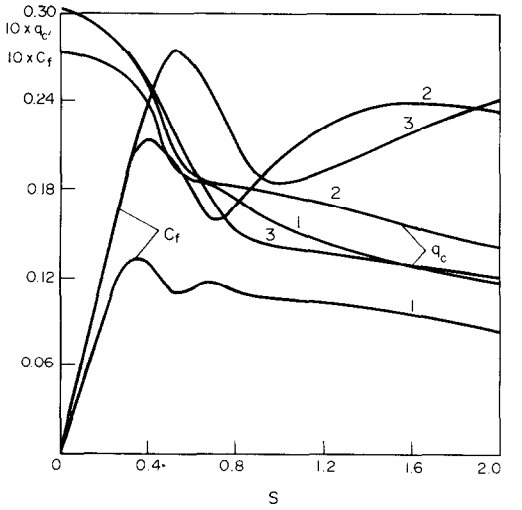

FIG. 3. Convective heat flux and skin friction coefficient distributions along the cones with different half-angles for $v_\infty = 6000$ m/s; $\rho_\infty = 2 \times 10^{-4}$ kg/m^3; $a = 0.2$ m; $T_w = 2500$ K.

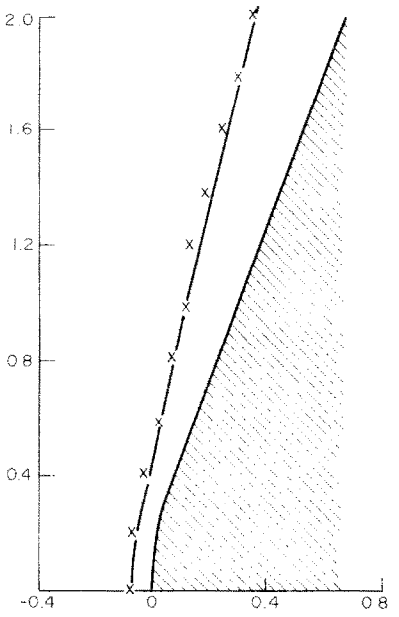

FIG. 4. Comparison of shock detachment distance with experimental results of Miller and Moore [22] for $v_\infty = 5000$ m/s; $\rho_\infty = 4.74 \times 10^{-3}$ kg/m^3; $a = 0.0127$ m; $T_w = 3000$ K.

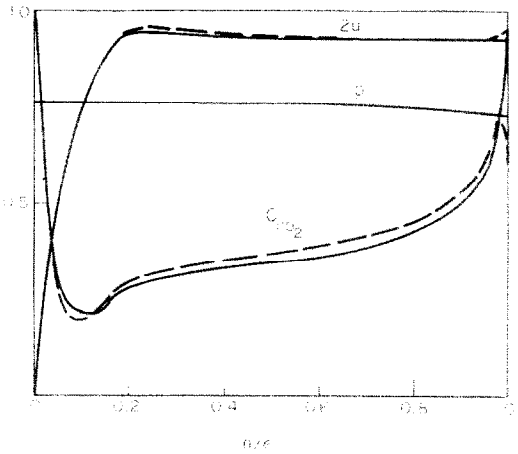

FIG. 6. Comparison of calculated shock layer parameters and the results of [12] for $v_\infty = 5500$ m/s; $\rho_\infty = 3.83 \times 10^{-4}$ kg/m^3; $a = 1$ m; $\theta_c = 60°$; $s = 1.57$; $T_w = 1000$ K.

presented in Figs. 1–6 is estimated to be within a few percent which conforms to the accuracy of the available data on chemical kinetics.

The calculation results are presented in dimensionless form. Linear dimensions are related to the body nose radius, pressure—to $\rho_\infty v_\infty^2$, heat fluxes—to $\rho_\infty v_\infty^3$, specific vibrational energy of carbon dioxide molecules—to v_∞^2, temperature—to $m_\infty v_\infty^2/2R$. The skin friction coefficient is defined as a ratio of the shear stress on the body surface to $\rho_\infty v_\infty^2/2$.

The results presented in Figs. 1–6 are obtained for pure carbon dioxide flows. The shock layer parameters on the stagnation line are plotted in Fig. 1. Solid curves show the profiles calculated with vibrational relaxation of CO_2 taken into account, dash curves—under the assumption of vibrational equilibria. This figure also shows the concentration profiles of element C which are evaluated with the use of two models of multicomponent diffusion. According to the first model all of the mixture components are classified into three groups and the diffusion properties of the components within a single group are postulated to be identical. Thus, six different binary diffusion coefficients and three molecular weights were used in evaluating the diffusion fluxes. The results of this calculation are shown by a dash–dotted curve. The solid line corresponds to the use of the effective Schmidt numbers $Sc_i = 0.5$ for all of the mixture components. The figure clearly shows that a more precise description of the multicomponent diffusion hardly changes the results. The convective heat flux

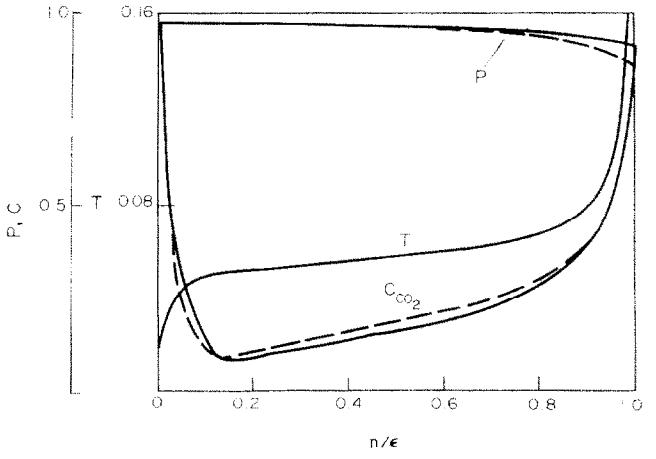

FIG. 5. Comparison of shock layer parameters and the numerical results of Afonina and Gromov [12] for $v_\infty = 5500$ m/s; $\rho_\infty = 3.83 \times 10^{-4}$ kg/m^3; $a = 1$ m; $\theta_c = 60°$; $s = 0$; $T_w = 1000$ K.

and the skin friction coefficient differ by only a few percent.

Some results of calculation of flows about the cones with different half-angles are depicted in Figs. 2 and 3. Curves 1, 2 and 3 correspond to $\theta_c = 70$, 60 and 50°. The quantity C_{co}^m denotes the maximum of the carbon monoxide concentration on the line $s = \text{const}$. It is seen from Fig. 2 that the flow past a cone with $\theta_c = 70°$ is characterized by a significant increase in the shock layer thickness. In this case the concentration of species along the shock layer varies non-monotonically. Comparison of calculated shock wave location for the cone having the half-angle $\theta_c = 70°$ with the experimental data of Miller and Moore [22] is presented in Fig. 4.

In Figs. 5 and 6, the profiles of gasdynamic functions and carbon dioxide concentration are compared with the numerical results obtained by Afonina and Gromov [12] who used a shock capturing method to solve the Navier–Stokes equations. Dashed curves in these figures correspond to their solution.

In order to study the effect of impurities on the shock layer parameters, the following mixtures have been used: 73% CO_2 + 27% Ar and 95% CO_2 + 5% N_2 (by volume). In the first case a notable (15–20%) increase of the shock layer thickness and temperature has been revealed. Nitrogen added in the amount of 5% markedly affects the species concentrations only. Pressure, convective heat flux and skin friction coefficient do not differ more than by a few percent.

3. ESTIMATES OF RADIATIVE HEATING

Available theoretical and experimental data [23] show that under the conditions considered non-equilibrium shock layer radiation of $CO_2 + N_2 + Ar$ mixtures is mainly controlled by electronic transitions in carbon monoxide and cyanogen molecules, namely, by the CO^{4+}, CN violet and CN red band systems. The lack of the necessary information on the kinetics of electronic excitation does not permit an exact analysis of non-equilibrium shock layer radiation. Therefore all that will be given here are some estimates of radiative heating of the surfaces of bodies. To this end, a simple two-level model of non-equilibrium radiation [24] is used. The parameters of electronic states are borrowed from [25]. The concentrations of the excited molecules are determined by integration of the respective stationary continuity equations. The requisite data on the flow field parameters are taken from the numerical solution of the previous Section. This solution is assumed to provide the concentration of molecules in the ground electronic state. The effective Schmidt number for excited molecules is assumed to be 0.5. The production rate of the excited molecules is determined with account for two-body collisions and radiative processes. Because of lack of data on collisional quenching cross-sections for the electronic states $CO(A^1\Pi)$, $CN(B^2\Sigma^+)$ and $CN(A^2\Pi_i)$, these are assumed to be equal to the gas-kinetic one ($\sigma = 10^{-15}$ cm^2), which allows upper estimation of radiative heating. In such a procedure, one may neglect electron impact excitations, the quenching cross section of which is about 10^{-17} cm^2, according to [26].

The radiative production rate of the excited molecules is determined from the solution of the radiation transport equation in the approximation of a one-dimensional tangent slab [24]. This approximation is also applied for evaluation of the radiative heat flux to the body surface. The values of the absorption cross sections are taken from tables of [25]. For other details see [6, 19].

The continuity equations for excited molecules are the equations of a parabolic type. The boundary conditions at the detached shock wave are formulated in the same manner as in the previous Section. The concentration of the excited molecules at the body surface is assumed to be equal to the value in a state of equilibrium at the wall temperature. On the stagnation line the problem is reduced to the ordinary differential equations that are solved numerically. To obtain the solution along the body surface the implicit finite-difference scheme of Crank–Nicholson type is used. Iterations are applied to account for the reabsorption of radiation.

Some results are depicted in Figs. 7–9. Figure 7 shows the dependence of the convective and radiative heat fluxes at the forward stagnation point on the ambient density for initial mixture composition 95% CO_2 + 5% N_2 (by volume). The contributions of CO^{4+}, CN violet and CN red band systems are shown by curves 1, 2, 3. Dash curves correspond to the equilibrium values of convective and total radiative heat fluxes. Nonequilibrium radiative heating significantly exceeds the equilibrium values and this is in qualitative agreement with the available experimental data [23]. It is also seen from Fig. 7 that under the

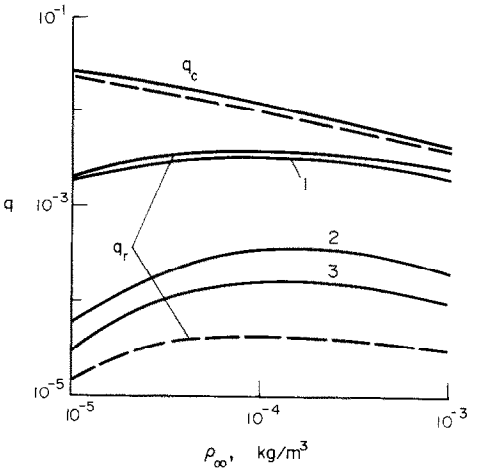

FIG. 7. Convective and radiative heat fluxes at the stagnation point vs ambient density for $v_\infty = 6000$ m/s; $a = 1$ m; $\theta_c = 60°$; $T_w = 2900$ K.

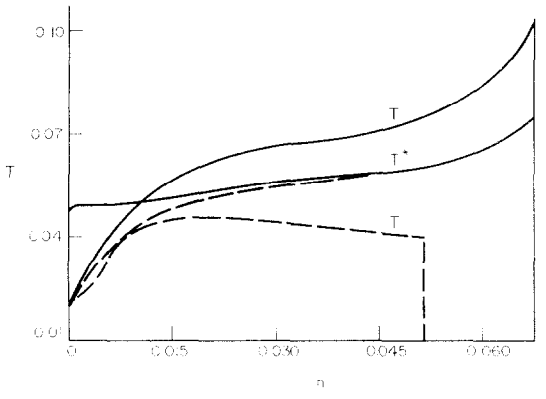

FIG. 8. Temperature profiles for $v_\infty = 7000$ m/s; $\rho_\infty = 2.07 \times 10^{-4}$ kg/m^3; $a = 0.2$ m; $\theta_c = 60°$; $s = 0.524$; $T_w = 2500$ K.

assumptions accepted above for the electronic excitation kinetics it is quite possible to consider the radiation of the fourth positive band system only to estimate the radiative heating of the body surface.

Figure 8 shows typical profiles of the translational temperature and the effective temperature of electronic excitation of carbon monoxide molecules

$$T^* = -\frac{E^*}{k \ln(g^\circ C^*/g^* C^\circ)}. \tag{7}$$

Dash curves indicate the translational temperature profile calculated under the assumption of local thermodynamic equilibrium and the profile of T^* evaluated under the assumption of transparency of the shock layer for CO^{4+} emission. It is seen that reabsorption notably affects the excited molecules concentration near the wall. The role of reabsorption in the electronic excitation kinetics of the CN molecules was found to be negligible.

It should be noted that at the adopted value of collisional quenching cross-section, only radiative processes violate the electronic equilibria. The effective temperature T^* calculated for non-radiating shock layer does not differ from the translational one.

Variation of the CO^{4+} radiative heat flux along the body surface is depicted by curve 1 in Fig. 9. Other solid curves in this figure show the radiative heat fluxes evaluated under the following assumptions: (2) optically thin shock layer; (3) $T^*_{CO} = T$; (4) local thermodynamic equilibrium. The dashed curve indicates the convective heat flux. It is clear that under the conditions considered the assumption on the local thermodynamic equilibrium is inadequate for evaluation of the radiative heating of body surface. The assumption that $T^* = T$ results in overestimation of the radiative heat flux. Account for the radiative processes in the electronic excitation kinetics yields more realistic values of q_r. The radiative heat flux turns then to be lower than the convective heat flux over the entire body surface.

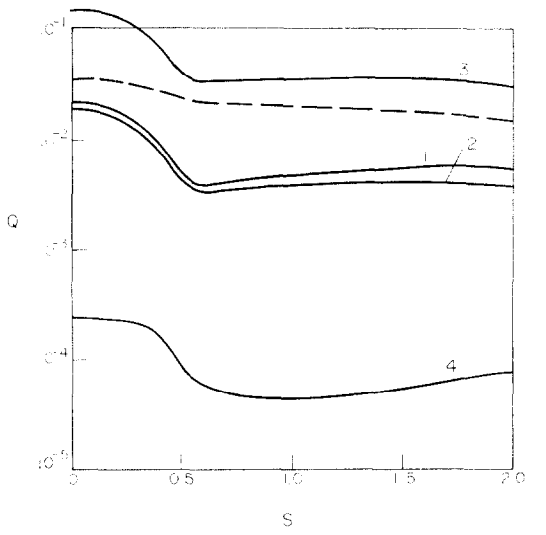

FIG. 9. Variation of heat fluxes along the body surface for $v_\infty = 7000$ m/s; $\rho_\infty = 2.07 \times 10^{-4}$ kg/m^3; $a = 0.2$ m; $\theta_c = 60°$; $T_w = 2500$ K.

4. ANALYSIS OF NONEQUILIBRIUM IONIZATION

In the study of nonequilibrium shock layer ionization the mixture is assumed to be quasi-neutral. Ambipolar diffusion is described by means of the constant effective Schmidt number. The distributions of gas-dynamic functions and of neutral species obtained in Section 2 are used. Under the conditions considered, ionization of the shock layer occurs mainly due to collisions of heavy particles. Because of this fact and high efficiency of energy exchange between electrons and molecules it is possible to assume the electron temperature to be equal to the translational temperature of heavy particles [27].

Determination of the density of electrons reduces to the solution of a set of parabolic stationary continuity equations for ions. The problem is formulated and solved in the same manner as in the previous Section. The body surface is assumed to be non-conducting and catalytic as regards recombination of ions. An approximate wall boundary condition, $C_{iw} = 0$, is used the validity of which was demonstrated by Knight [28] and Nishida [29].

Ablation of some body surface materials results in appearance of sodium vapour in the shock layer. To account for its effect the continuity equation for element Na is solved. The corresponding wall boundary condition represents a balance between the diffusion flux of element Na to the body surface and its production rate due to ablation.

In preliminary calculations, 27 ionization and charge exchange processes were taken into consideration. A numerical analysis showed that the following reactions provide a main contribution (above 90%) to the electron density:

(1) $N+O \rightleftarrows NO^+ + e$, (6) $CO+CO^+ \rightleftarrows C^+ + CO_2$,
(2) $C+O \rightleftarrows CO^+ + e$, (7) $Na+M \rightleftarrows Na^+ + e + M$,
(3) $O+O \rightleftarrows O_2^+ + e$, (8) $O_2+Na^+ \rightleftarrows O_2^+ + Na$,
(4) $CO+NO^+ \rightleftarrows CO^+ + NO$, (9) $NO+Na^+ \rightleftarrows NO^+ + Na$,
(5) $CO+O^+ \rightleftarrows CO^+ + O$, (10) $CO+Na^+ \rightleftarrows CO^+ + Na$.

The rate constants for reactions (1)–(4) are taken from [18], for (5) and (6)—from [30] and for (7)–(10)—from [31, 32]. For pure carbon dioxide flows only reactions (2)–(6) are included in the analysis.

The calculation results are given in Figs. 10–14. The profiles of number density of electrons N_e (1/cm^3) on the stagnation line are shown in Fig. 10 for a pure carbon dioxide flow. These results demonstrate the influence of some assumptions accepted in the formulation of the problem. Thus, curves 1 and 2 correspond to two limiting cases of a catayltic and a non-catalytic wall as regards dissociation–recombination reactions. Solid and dashed lines 2 are the profiles of electron number density evaluated with the use of the ambioplar Schmidt numbers $Sc_a = 0.25$ and 0.5. It is seen that the N_e profile is only slightly influenced by variations in the catalytic properties of the body surface and ambipolar Schmidt numbers. All other calculations were performed for the case of a catalytic wall with the ambipolar Schmidt number equal to $Sc_a = 0.25$. The profiles of mass fractions of ions are plotted in Fig. 11.

To study the effect of thermal non-equilibria between electrons and heavy particles the calculation has been performed with the electron temperature assumed to be equal to the vibrational temperature of CO_2 molecules. A corresponding change in the electron density profile was found to be negligible.

The N_e profile calculated under the assumption of vibrational equilibria for all molecules is indicated by dash line 1. It is seen that there is a significant influence of carbon dioxide vibrational relaxation on the electron concentration in spite of rather a small length of the vibrational relaxation zone, see Fig. 1.

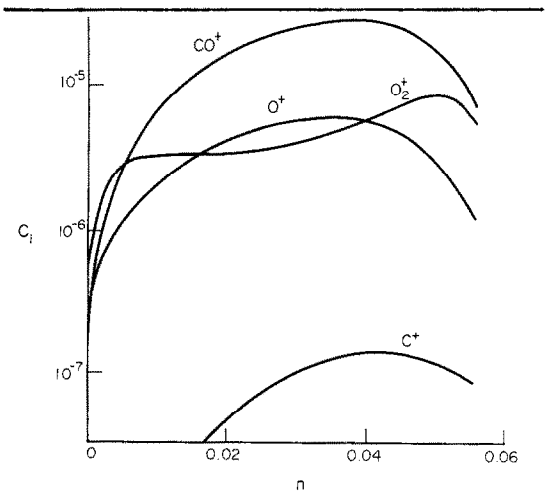

FIG. 11. Profiles of mass fractions of ions on the stagnation line for $v_\infty = 5500$ m/s; $\rho_\infty = 2.07 \times 10^{-4}$ kg/m^3; $a = 0.2$ m; $\theta_c = 60°$; $T_w = 1100$ K.

Profiles of the electron number density for various ambient density values are shown in Fig. 12 by curves 1, 2, 3 which correspond to $\rho_\infty = 3 \times 10^{-5}, 3 \times 10^{-4}$ and 3×10^{-3} kg/m^3. Evolution of the N_e profile illustrates a transition from frozen to equilibrium shock layer ionization. The maximum in the electron

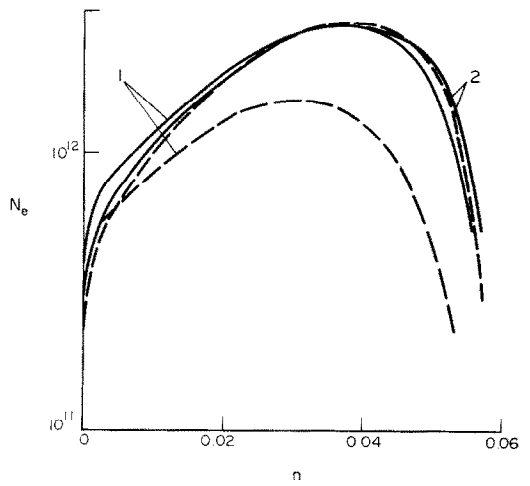

FIG. 10. Profiles of electron number density on the stagnation line for $v_\infty = 5500$ m/s; $\rho_\infty = 2.07 \times 10^{-4}$ kg/m^3; $a = 0.2$ m; $\theta_c = 60°$; $T_w = 1100$ K.

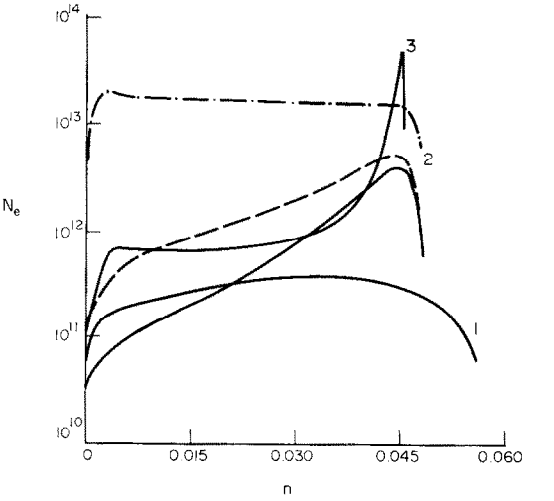

FIG. 12. Profiles of electron number density on the stagnation line for various ambient densities and initial mixture compositions, $v_\infty = 5500$ m/s; $a = 1$ m; $\theta_c = 60°$; $T_w = 1100$ K.

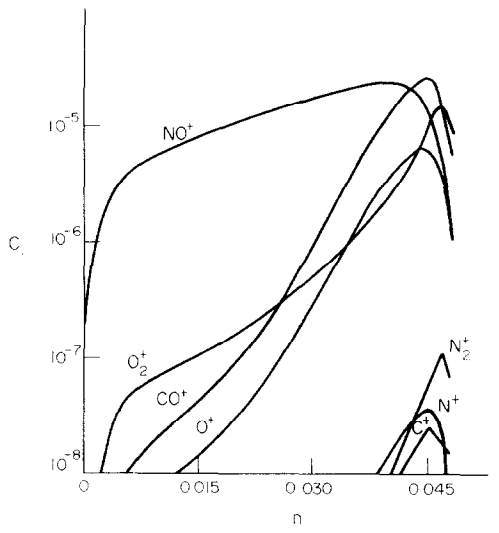

FIG. 13. Profiles of mass fractions of ions on the stagnation line for initial mixture composition 99% CO_2 + 1% N_2, v_∞ = 5500 m/s: $\rho_\infty = 3 \times 10^{-4}$ kg/m^3; a = 1 m; $\theta_c = 60°$; T_w = 1100 K.

density becomes more explicit and moves towards the shock front when the ambient density increases.

Solid curves in Fig. 12 show the results for a pure carbon dioxide free stream. Dash line 2 corresponds to the initial mixture composition 99% CO_2 + 1% N_2 (by mass). The profiles of mass fractions of ions for this case are plotted in Fig. 13. Dashed–dotted curve 2 in Fig. 12 shows the electron density profile evaluated with sodium impurity effect taken into account for the initial mixture composition 99% CO_2 + 1% N_2. According to the data presented in [18] the rate of element Na production at the body surface was assumed to be equal to 5×10^{-4} kg/m^{2}s. It is seen that there is a significant effect of impurities on the shock layer ionization.

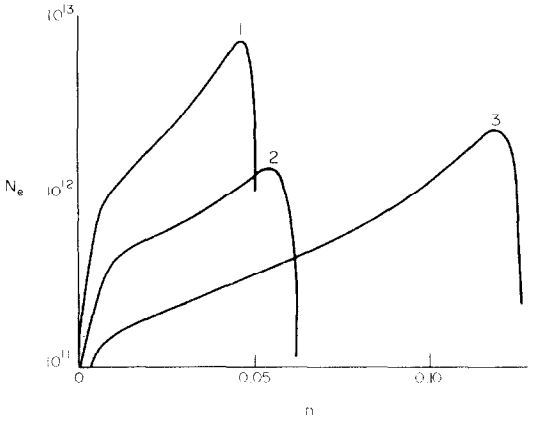

FIG. 14. Variation of electron number density profile along the shock layer for v_∞ = 5500 m/s; $\rho_\infty = 3 \times 10^{-4}$ kg/m^3; a = 1 m; $\theta_c = 60°$; T_w = 1100 K.

Evolution of the electron number density profile along the shock layer is shown in Fig. 14 for free stream mixture 98% CO_2 + 2% N_2. Curves 1, 2, 3 correspond to s = 0, 0.698 and 1.92. A non-monotonic variation of the N_e maximum along the shock layer is apparent.

5. CONCLUSIONS

Carbon dioxide flows about the blunted cones with large half-angles are numerically investigated for the Mars entry conditions. The flow field, skin friction and heat-transfer parameters as well as mixture components concentrations are calculated. The estimated values of the radiative heat flux to the body surface prove to be smaller than the convective heat flux values. The processes providing a main contribution to the shock layer ionization are revealed. A significant effect of the vibrational relaxation of carbon dioxide molecules as well as of nitrogen and sodium impurities on the electron concentration is demonstrated. The dependence of the flow field, heat transfer and electron density on the free stream parameters and the body shape is investigated.

REFERENCES

1. P. M. Chung, Hypersonic viscous shock layer of non-equilibrium dissociating gas, NASA TR R-109 (1961).
2. T. C. Dellinger, Computation of nonequilibrium merged stagnation shock layers by successive accelerated replacement, *AIAA J* **9**(2), 262–269 (1971).
3. V. G. Voronkin, Nonequilibrium viscous flow of multicomponent mixture in the stagnation region of a blunt body, *Izv. Akad. Nauk SSSR. Mekh.Zhidk. Gaza* No. 2, 144–147 (1971).
4. N. E. Afonina and V. G. Gromov, Numerical study of the stagnation point heat transfer for a sphere in hypersonic carbon dioxide flow, *Izv. Akad. Nauk SSSR. Mekh.Zhidk. Gaza* No. 1, 117–120 (1975).
5. A. Kumar and A. C. Jain, Nonequilibrium merged stagnation shock layers at hypersonic speeds, *Int. J. Heat Mass Transfer* **18**(10), 1113–1118 (1975).
6. Yu. P. Golovachov, Convective and radiative heat transfer in blunt body flows of nonequilibrium CO_2 + N_2 mixtures, *Teplofiz. Vysok. Temper.* **16**(5), 1109–1111 (1978).
7. R. T. Davis, Hypersonic flow of a chemically reacting binary mixture past a blunt body, AIAA Paper, No. 805 (1970).
8. T. C. Dellinger, Nonequilibrium air ionization in hypersonic fully viscous shock layer, AIAA Paper, No. 806 (1970).
9. C. P. Li, Hypersonic nonequilibrium flow past a sphere at low Reynolds numbers, AIAA Paper, No. 173 (1974).
10. C. D. Scott, Reacting shock layers with slip and catalytic boundary conditions, *AIAA Jl* **13**(10), 1271–1278 (1975).
11. E. W. Miner and C. H. Lewis, Hypersonic ionizing air viscous shock layer flows over sphere-cones, *AIAA Jl* **13**(1), 80–88 (1975).
12. N. E. Afonina and V. G. Gromov, Viscous carbon dioxide flow about a blunted cone, *Izv. Akad. Nauk SSSR, Mekh. Zhidk. Gaza* No. 4, 102–105 (1978).
13. Yu. P. Golovachov, A. M. Kuzmin and F. D. Popov, On the calculation of supersonic blunt body flow on the basis of complete and simplified Navier–Stokes equations, *Zh. Vych. Mat. Mat. Fiz.* **13**(4), 1021–1028 (1973).
14. R. L. Taylor and S. Bitterman, Survey of vibrational relaxation data for processes important in the CO_2 + Ar laser systems, *Rev. Mod. Phys.* **41**(1), 26–47 (1969).
15. K. C. Yun and E. A. Mason, Collision integrals for the

transport properties of dissociating air at high temperature, *Physics Fluids* **5**(4), 380–386 (1962).
16. A. P. Kalinin, V. B. Leonas and A. V. Sermyagin, Collision integrals for the components of dissociating planetary atmospheres, *Teplofiz. Vysok. Temper* **9**(5), 1066–1068 (1971).
17. R. L. McKenzie and J. O. Arnold, Experimental and theoretical investigations of the chemical kinetics and nonequilibrium CN radiation behind shock waves in $CO_2 + N_2$ mixtures, AIAA Paper No. 322 (1967).
18. J. C. Evans, C. J. Schexynayder and W. L. Grose, Effects of nonequilibrium ablation chemistry on Viking radio blackout, *J. Spacecraft Rockets* **11**(2), 84–88 (1974).
19. Yu. P. Golovachov and Yu. P. Lunkin, Flow about a planetary entry vehicle, *Acta Astronautica* **6**(3), 541–555 (1979).
20. Yu. P. Golovachov, Calculation of supersonic blunt body flow of nonequilibrium mixtures on the basis of Navier–Stokes equations, *Zh. Vych. Mat. Mat. Fiz.* **18**(5), 1266–1274 (1978).
21. Yu. P. Golovachov and F. D. Popov, Hypersonic flow of a viscous radiating gas past blunt cones, *Inzh.-Fiz. Zh.* **29**(5), 864–869 (1975).
22. C. G. Miller and J. A. Moore, Shock shapes of blunt bodies in hypersonic helium, air and CO_2 flows, *AIAA Jl* **12**(3), 411–413 (1974).
23. R. Goulard, R. E. Boughner, R. K. Burns and H. F. Nelson, Radiating gas flows during planetary entry, *Teplofiz. Vysok. Temper.* **7**(3), 542–565 (1969).
24. S.-I.-Pai, *Radiation Gas Dynamics.* Springer, Berlin (1966).
25. V. A. Kamenschikov, Yu. A. Plastinin, V. M. Nikolayev and L. A. Novitsky, *Radiative Properties of High-Temperature Gases.* Mashinostroeniye, Moscow (1970).
26. M. J. Mumma, E. J. Stone and E. C. Zipf, Excitation of the CO fourth positive band system by electron impact on carbon monoxide and carbon dioxide, *J. Chem. Phys.* **54**(6), 2627–2634 (1971).
27. L. M. Biberman, A. H. Mnatsakanyan and I. T. Yakubov, Ionization relaxation behind strong shock waves in gases, *Usp. Fiz. Nauk* **103**(3), 431–462 (1970).
28. D. D. Knight, Electron thermochemical nonequilibrium effects in re-entry boundary layers, *AIAA Jl* **9**(2), 193–199 (1971).
29. M. Nishida, Nonequilibrium viscous shock layer in a partially ionized gas, *Physics Fluids* **15**(4), 596–602 (1972).
30. M. G. Dunn, Measurement of $C^+ + e + e$ and $CO^+ + e$ recombination in carbon monoxide flows, *AIAA Jl* **9**(11), 2184–2191 (1971).
31. D. E. Jensen, Comment on "Effects of nonequilibrium ablation chemistry on Viking radio blackout", *J. Spacecraft Rockets* **11**(10), 736–737 (1974).
32. A. L. Farragher, J. A. Peden and W. L. Fite, Charge transfer of N_2^+, O_2^+ and NO^+ to sodium atoms at thermal energies, *J. Chem. Phys.* **50**(1), 287–293 (1969).

ETUDE NUMERIQUE DE L'ECOULEMENT SUPERSONIQUE ET HORS D'EQUILIBRE DU GAZ CARBONIQUE AUTOUR D'OBSTACLES

Résumé—L'écoulement axisymétrique hors d'équilibre autour de cones ayant un nez sphérique est étudié à partir des équations de Navier–Stokes. On prend en compte la relation vibrationnelle des molécules de gaz carbonique, la physico-chimie des états hors d'équilibre et le transfert d'énergie par rayonnement. Les solutions numériques sont obtenues par utilisation d'une méthode implicite aux différences finies. On étudie l'effet des impuretés d'azote, d'argon et de sodium sur les paramètres de la couche de choc.

NUMERISCHE UNTERSUCHUNG EINER ÜBERSCHALL-NICHTGLEICHGEWICHTS-STRÖMUNG VON KOHLENDIOXID UM STUMPFE KÖRPER

Zusammenfassung—Auf der Grundlage der Navier–Stokes-Gleichungen wird die achsensymmetrische Strömung um kugelförmig abgerundete Kegel untersucht. Schwingungsrelaxation der Kohlendioxidmoleküle, Nichtgleichgewichtsreaktionen und Strahlungswärmeaustausch werden berücksichtigt. Lösungen werden numerisch unter Verdwendung von impliziten finiten Differenzenverfahren ermittelt. Der Einfluß von Stickstoff-, Argon- und Natrium-Verunreinigungen auf die Stoßfront-Parameter wurde untersucht.

ЧИСЛЕННОЕ ИССЛЕДОВАНИЕ СВЕРХЗВУКОВОГО НЕРАВНОВЕСНОГО ОБТЕКАНИЯ ЗАТУПЛЕННЫХ ТЕЛ УГЛЕКИСЛЫМ ГАЗОМ

Аннотация — На основе уравнений Навье–Стокса рассматривается неравновесное осесимметричное обтекание сферически затупленных конусов. Учитывается колебательная релаксация молекул CO_2, неравновесное протекание химических реакций и радиационный перенос энергии. Решение задачи находится численно с помощью неявных конечно-разностных схем. Исследуется влияние примесей азота, аргона и натрия на параметры ударного слоя.